

Spin-triplet pair density wave superconductors

Yi Zhang^{1,2,*} and Ziqiang Wang^{3,†}

¹*Department of Physics and Institute for Quantum Science and Technology, Shanghai University, Shanghai 200444, China*

²*Shanghai Key Laboratory of High Temperature Superconductors and International Center of Quantum and Molecular Structures, Shanghai University, Shanghai 200444, China*

³*Department of Physics, Boston College, Chestnut Hill, MA 02467, USA*

(Dated: August 27, 2024)

Recent experiments have shown that the nonzero center of mass momentum pair density wave (PDW) is a widespread phenomenon observed over different superconducting materials. However, concrete theoretical model realizations of the PDW order have remained elusive. Here, we study a one-dimensional model with nearest-neighbor pairing attraction, i.e. a spinful Kitaev chain, under generic spin-orbit couplings such that the spin-rotation symmetry is fully broken. The most general superconducting order parameter is described by a spatial dependent \mathbf{d}_i -vector. We show that a spin-triplet pair density wave (t-PDW) emerges in the ground state and occupies a large part of the phase diagram. The \mathbf{d}_i -vector of the t-PDW rotates with a pitch Q_{pdw} along the chain and spans an ellipsoid. The pure t-PDW is fully-gapped and a class-DIII topological superconductor with two Majorana zero modes localized at each end of the chain and protected by time-reversal symmetry. Our findings reveal unprecedented insights into the exotic pure PDW superconductor and provide a possible explanation for the one-dimensional PDW detected along domain walls in monolayer iron-based superconductor Fe(Te,Se) and potentially realizable using other quantum structures in unconventional superconductors.

In the conventional BCS theory of superconductors, electrons occupying time-reversed quantum states pair together to form Cooper pairs with zero center-of-mass momentum, giving rise to a uniform superconducting order parameter that respects translation symmetry [1]. However, in a magnetic field that breaks the time-reversal symmetry, it was proposed that the Cooper pairs can acquire a finite center-of-mass momentum and give rise to the Fulde–Ferrell–Larkin–Ovchinnikov (FFLO) superconductor [2, 3] with a spatially modulated superconducting (SC) order parameter.

The FFLO states can be further divided into FF and LL states. The Cooper pairs in the FF state carry a single nonzero momentum \mathbf{q} , such that the SC order parameter breaks time-reversal symmetry and varies in space as $\Delta(\mathbf{r}) = \Delta_{\mathbf{q}} e^{i\mathbf{q}\cdot\mathbf{r}}$. This helical superconductor has been extensively studied in noncentrosymmetric systems with spin-orbit coupling (SOC) and time-reversal symmetry-breaking fields [4–17]. It is believed to play an important role in realizing the diode effect in SC systems [18–20]. The LO state, on the other hand, is described by a SC order parameter containing at least two nonzero momenta i.e., $\pm\mathbf{q}$, and varies in space according to $\Delta(\mathbf{r}) = \Delta_{\mathbf{q}} \cos(\mathbf{q} \cdot \mathbf{r})$. This inhomogeneous SC state does not require broken time-reversal symmetry. Its generalization in the absence of an external magnetic field is more commonly referred to as the pair density wave (PDW) state [21].

The PDW state has been proposed to exist in the high- T_c cuprate superconductors [22–33] and has attracted intense research interest [34–70]. More recently, evidence for PDW formation has been reported in iron-based superconductors [71, 72], heavy-fermion superconductors [73, 74], and kagome superconductors [75, 76]. Despite these exciting developments, concrete theoretical model realizations of the

PDW states beyond phenomenological Landau free-energy descriptions have remained very challenging.

Motivated by the recent experimental progress, especially the detection of the one-dimensional PDW modulations at the domain walls in the iron-based superconductor Fe(Te,Se) film [72], we propose and study a one-dimensional (1D) model with nearest-neighbor pairing attraction and spin-orbit couplings (SOCs) such that the spin-rotation symmetry is fully broken. This simple and concrete model can be thought as a spinful Kitaev chain in the presence of both Rashba (α_R) and Dresselhaus (α_D) SOC. Since the spin rotation symmetry is fully broken, the pairing interaction can be parametrized independently by attractions in the equal-spin (V_1) and opposite-spin (V_2) channels. The nature of the SC states can thus be explored by varying the ratio of $r_V = V_2/V_1$ and $r_{\text{so}} = \alpha_D/\alpha_R$.

Due to the broken inversion symmetry, the pairing state is in general of a mixed parity type, with the spin-triplet sector specified by the d -vector [77]. The most general SC state can thus be described by a spatial-dependent pairing order parameter (Methods)

$$\Delta_{i,\sigma\sigma'} = [(\psi_i\sigma_0 + \mathbf{d}_i \cdot \boldsymbol{\sigma})i\sigma_y]_{\sigma\sigma'} \quad (1)$$

where ψ_i and \mathbf{d}_i correspond to the spin-singlet and the spin-triplet components at site- i , respectively. We perform self-consistent mean-field theory calculations and explore the phase diagram as a function of the SOC ratio r_{so} and the ratio of opposite and equal-spin attractions r_V . We find that a time-reversal symmetric, spin-triplet pair density wave (t-PDW) superconductor emerges in the ground state and occupies a large part of the phase diagram, which also contains a uniform mixed-parity (MP) superconductor. For a fixed SOC ratio r_{so} , the phase diagram is shown schematically shown in Fig. 1, displaying a transition from the uniform MP topological superconductor (TSC) for $V_2 > V_1$ to a t-PDW TSC for $V_1 > V_2$. In the t-PDW phase, the spin-singlet component vanishes, while the \mathbf{d}_i -vector rotates with a pitch Q_{pdw} along the chain and spans an ellipsoid (Fig. 1). We will

* zhangyi821@shu.edu.cn

† ziqiang.wang@bc.edu

show that this pure t-PDW is fully-gapped and belongs to the class-DIII TSC with two Majorana zero modes localized at each end of the chain and protected by time-reversal symmetry. Moreover, we study the evolution of the phase diagram with the chemical potential and the properties of the topological phase transitions. Our simple and concrete model allows us to address the critical question of how the pairing interaction and SOC work together to overcome the kinetic energy of the pairs with nonzero center of mass momentum, such that the t-PDW can emerge in the ground state.

Results

Model

The Hamiltonian of our 1D model of a spin-orbit coupled chain with nearest neighbor (nn) attraction is given by

$$\hat{H} = \sum_{i\sigma\sigma'} c_{i\sigma}^\dagger (-t\sigma_0 + i\alpha_R\sigma_z + i\alpha_D\sigma_x)_{\sigma\sigma'} c_{i+1\sigma'} + h.c. - V_1 \sum_{i\sigma} n_{i\sigma} n_{i+1\sigma} - V_2 \sum_{i\sigma} n_{i\sigma} n_{i+1\bar{\sigma}} \quad (2)$$

where t is the nn hopping parameter, α_R , and α_D describe the nn Rashba and Dresselhaus SOC, and V_1 and V_2 are the attractions between equal-spin and opposite-spin charge densities on the nn sites, respectively.

This effective Hamiltonian can describe the embedded quantum structures in high- T_c superconductors due to spatial symmetry breaking [78], such as along the atomic line defects in monolayer Fe(Te,Se) [79]. The effective attraction V_1 and V_2 can be different since the system already breaks the spin rotation symmetry. Here, the interaction term breaks SU(2) spin rotation symmetry down to U(1) symmetry about z axis when $V_1 \neq V_2$, while the SOC term breaks the SU(2) symmetry down to U(1) symmetry about a general axis determined by α_R and α_D , therefore the Hamiltonian fully breaks the spin rotation symmetry, which is important to realize the PDW state. The two attraction terms can be decomposed into equal-spin and opposite-spin pairing channels so that the full Hamiltonian can be written as

$$\hat{H} = \sum_{k,\sigma\sigma'} c_{k\sigma}^\dagger [h_0(k)]_{\sigma\sigma'} c_{k\sigma'} - N_c V_1 \sum_{q\sigma} \hat{\Delta}_{\parallel,q,\sigma}^\dagger \hat{\Delta}_{\parallel,q,\sigma} - N_c V_2 \sum_{q\sigma} \hat{\Delta}_{\perp,q,\sigma}^\dagger \hat{\Delta}_{\perp,q,\sigma} \quad (3)$$

where the pairing operators in the two channels are defined as

$$\begin{cases} \hat{\Delta}_{\parallel,q,\sigma} = \frac{1}{N_c} \sum_k i \sin kc_{-k+\frac{q}{2}\sigma} c_{k+\frac{q}{2}\sigma} \\ \hat{\Delta}_{\perp,q,\sigma} = \frac{1}{N_c} \sum_k e^{-ik} c_{-k+\frac{q}{2}\bar{\sigma}} c_{k+\frac{q}{2}\sigma} \end{cases} \quad (4)$$

and the non-interacting Hamiltonian is written as

$$h_0(k) = (-2t \cos k - \mu)\sigma_0 - 2 \sin k(\alpha_R\sigma_z + \alpha_D\sigma_x) \quad (5)$$

Here, k is the momentum, μ is the chemical potential, $\{\sigma_0, \sigma_x, \sigma_y, \sigma_z\}$ are the identity matrix, and three Pauli matrices in the spin space and N_c is the number of sites. $h_0(k)$ describes the bare bands splitted by SOC as shown schematically in Fig. 2.

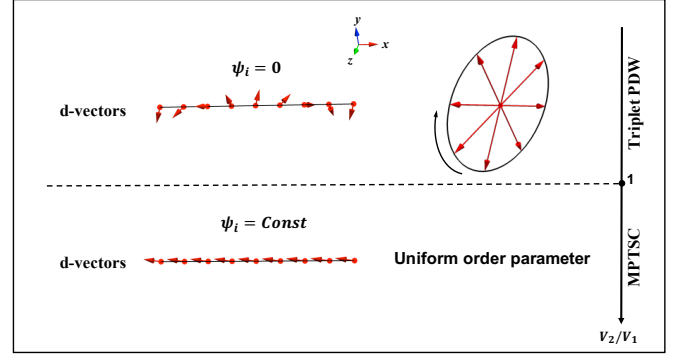


FIG. 1. **Triplet PDW state.** Schematic phase diagram as the ratio of the attraction $r_V = \frac{V_2}{V_1}$ is tuned for a small value of the ratio of spin-orbit coupling $r_{so} = \frac{\alpha_D}{\alpha_R}$. The phase transition between the t-PDW state and the uniform mixed-parity TSC (MPTSC) state occurs at the transition point with $V_1 = V_2$. The t-PDW state is a pure spin-triplet pairing state that can be described by a spatial-dependent imaginary d -vector. Its imaginary part is depicted by red arrows showing the spatial modulation. The d -vector revolves around the origin in an elliptical orbit in 3D space within a period of the t-PDW state. The uniform order parameters describe the MPTSC, i.e. both ψ and \mathbf{d} are uniform in real space.

Pairing order parameters

Due to the presence of both α_R and α_D , the wave function of each branch of the band contains both spin components, therefore, based on the structure of the Fermi surface shown in Fig. 2, the most general mean-field ansatz that respects the time-reversal symmetry can be written as

$$\begin{cases} \langle \hat{\Delta}_{\parallel,0,\uparrow} \rangle = \langle \hat{\Delta}_{\parallel,0,\downarrow} \rangle^* = \Delta_{\parallel,0}, & \langle \hat{\Delta}_{\perp,0,\uparrow} \rangle = -\langle \hat{\Delta}_{\perp,0,\downarrow} \rangle^* = \Delta_{\perp,0} \\ \langle \hat{\Delta}_{\parallel,Q,\uparrow} \rangle = \langle \hat{\Delta}_{\parallel,-Q,\downarrow} \rangle^* = \Delta_{\parallel,Q}, & \langle \hat{\Delta}_{\perp,Q,\uparrow} \rangle = -\langle \hat{\Delta}_{\perp,-Q,\downarrow} \rangle^* = \Delta_{\perp,Q} \\ \langle \hat{\Delta}_{\parallel,-Q,\uparrow} \rangle = \langle \hat{\Delta}_{\parallel,Q,\downarrow} \rangle^* = \Delta_{\parallel,-Q}, & \langle \hat{\Delta}_{\perp,-Q,\uparrow} \rangle = -\langle \hat{\Delta}_{\perp,Q,\downarrow} \rangle^* = \Delta_{\perp,-Q} \end{cases} \quad (6)$$

Here, the electrons belonging to the opposite branches can form Cooper pairs with zero center of mass momentum. Since each branch of the bands contains both spin components, the pairing can be either equal-spin pairing $\Delta_{\parallel,0}$ or opposite-spin pairing $\Delta_{\perp,0}$. While the equal-spin pairing must be spin-triplet, the opposite-spin pairing is in general mixed-parity pairing where the mixture of the spin-singlet and triplet pairing is controlled by the phase of the order parameter $\Delta_{\perp,0}$, with phase 0 corresponding to the s -wave pairing and phase $\pi/2$ corresponding to the p -wave pairing and other phase values corresponding to the mixture of both. On the other hand, the electrons belonging to the same branch can pair up with the nonzero center of mass momentum Q and $-Q$, which is determined by the SOC as $Q = 2 \arctan\left(\frac{\sqrt{\alpha_R^2 + \alpha_D^2}}{t}\right)$. Due to the same reason, the finite momentum intra-branch pairing can also be in the equal-spin ($\Delta_{\parallel,Q}$, $\Delta_{\parallel,-Q}$) and opposite-spin pairing channels ($\Delta_{\perp,Q}$, $\Delta_{\perp,-Q}$). The mean-field equations are then solved with a fixed chemical potential μ in the folded Brillouin Zone (BZ) for the commensurate Q . Assuming $Q = \frac{\pi}{D}$, the BZ is folded into $\frac{1}{2D}$ of the original BZ.

Full Phase diagram

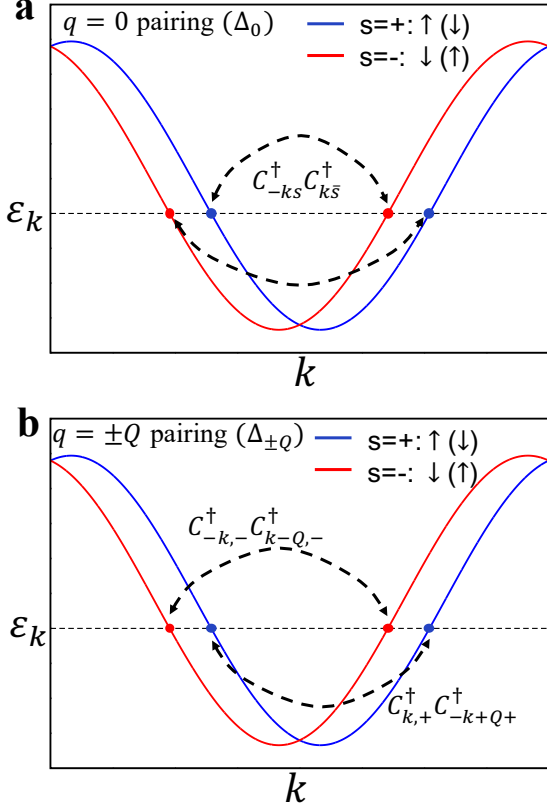


FIG. 2. **Schematic band structure of the spin-orbit coupled chain, showing different pairing channels across the Fermi points.** **a** The inter-branch pairing leads to the uniform pairing order with zero center of mass momentum for the Cooper pair $q=0$ (Δ_0). **b** The intra-branch pairing gives rise to the pairing states with the finite center of mass momentum $q=\pm Q$ ($\Delta_{\pm Q}$). Both pairings can be equal-spin and opposite-spin states.

We first choose the parameters as $t = 1$, $\mu = -0.4$, $\sqrt{V_1^2 + V_2^2} = 1.5$, $\sqrt{\alpha_R^2 + \alpha_D^2} = \tan(\pi/8)$, so that $Q = \frac{\pi}{4}$ and tune the ratio r_{so} and r_V . The ground state should be determined by comparing the energy of possible mean-field solutions and we find that the two most competitive states are the t-PDW state and the uniform MP state. The obtained phase diagram as functions of r_{so} and r_V are shown in Fig. 3, where two phase boundaries separate the t-PDW and MP states and cross at a single point. The phase diagram has several features. First of all, when $r_{so} = 0$, the ground state is always the Kramers Fulde-Ferrell (KFF) state for $r_V < 1$ until it reaches the transition point at $r_V = 1$ and the system transits to the MP state through a first-order phase transition which is studied in the previous work [20]. The KFF can be viewed as a special limit of the t-PDW state, where the Cooper pairs carry opposite momenta in the opposite spin channels. It has no spatial modulation in the local density of states, although its pairing function carries the finite center of mass momenta. This can be proved by connecting the KFF state to a uniform p -wave superconductor through a gauge transformation [20]. For the case with $r_V < 1$, introducing finite r_{so} invalidates such gauge

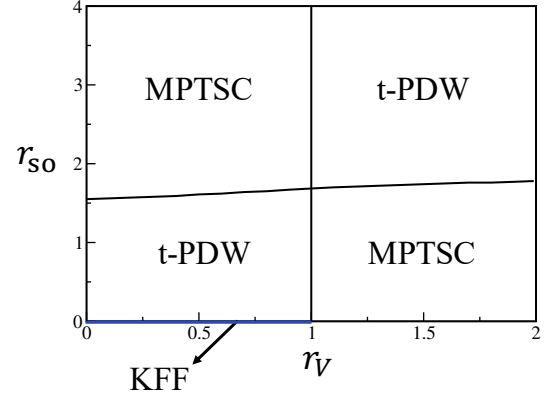


FIG. 3. **Phase diagrams close to half filling.** The t-PDW and MPTSC states are realized by tuning the two ratios r_{so} and r_V in the mean-field calculations, where the chemical potential $\mu = -0.4$ close to half filling. The KFF state is realized in the x -axis with $r_{so} = 0$ and $r_V < 1$ represented by the bold blue line.

transformation so that the ground state becomes the t-PDW state where the spatial modulation of the order parameters can no longer be gauged away. As r_{so} further increases, the system goes through a first-order phase transition and the ground state becomes the uniform MP state. Moreover, for the case with $r_V > 1$, the ground state remains the uniform MP state when the finite r_{so} is introduced until the ratio is big enough to induce a first-order transition from the MP state to the t-PDW state. While the horizontal transition line is determined numerically, the vertical transition line can be determined analytically and is verified in the numerical calculation.

This vertical transition line corresponds to the case with $r_V = 1$, where the interaction part of the Hamiltonian has the full SU(2) spin rotation symmetry. Then for the 1D system, the SOC reduces this symmetry to the U(1) symmetry corresponding to the spin rotation around the special axis with unit vector $\hat{n}_\alpha = (\alpha_D, 0, \alpha_R) / \sqrt{\alpha_R^2 + \alpha_D^2}$. Then we can always choose the spin quantization axis along the axis \hat{n}_α and the Hamiltonian thus becomes

$$\hat{H} = \sum_{i\sigma\sigma'} c_{i\sigma}^\dagger \left(-t\sigma_0 + i\sqrt{\alpha_R^2 + \alpha_D^2}\sigma_z \right)_{\sigma\sigma'} c_{i+1\sigma'} + h.c. - V_1 \sum_{i\sigma\sigma'} n_{i\sigma} n_{i+1\sigma'} \quad (7)$$

which corresponds to the transition points at $(r_{so} = 0, r_V = 1)$ in the phase diagram, where the KFF state and MP state are degenerate. Therefore, we can conclude that along the line with $r_V = 1$, the finite momentum pairing state and the uniform MP state are always degenerate, and the system will go through a first-order phase transition by crossing this line.

To understand the horizontal phase transition line, we can start with the left bottom of the phase diagram in Fig. 3. In this region where $r_V < 1$, the equal-spin pairing state is favored over the opposite-spin pairing state. Moreover, since α_R dominates over α_D in this region, each branch of the Fermi surface mainly consists of the same spin polarization, which

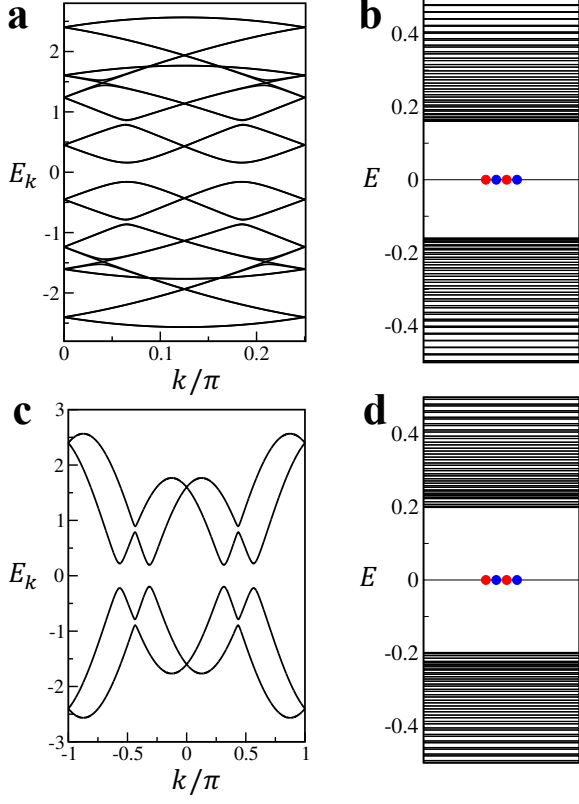


FIG. 4. **Properties of typical t-PDW and MP states shown in the phase diagram of Fig. 3.** **a,c** The band dispersion of t-PDW (**a**) and MP (**c**) states, where that of the t-PDW state is plotted in the folded Brillouin zone. **b,d** The energy spectrum obtained in a finite-size system with $L=320$, hosting four zero-energy MZMs denoted by blue and red dots. The parameters used are $r_{so}=1.4$ and $r_V=0.3$ for the t-PDW state and $r_{so}=3.0$ and $r_V=0.3$ for the MP state with $\mu = -0.4$ and all other parameters mentioned in the main text.

means the equal-spin pairing is mainly contributed by the intra-branch pairing as shown schematically in Fig. 2b, leading to the t-PDW state. Next, as α_D increases, which enhances the mixture of the two spin components within each branch of the Fermi surface, more contribution of the equal-spin pairing comes from the inter-branch pairing with zero center-of-mass momentum as depicted in Fig. 2a. Therefore, the system is driven into a uniform MP state. Contrarily, if we start from the right bottom of the phase diagram, where $r_V > 1$ and α_D dominates over α_R , the opposite-spin pairing is favored which mainly comes from the inter-branch pairing giving rise to the uniform MP state. Then increasing α_D drives the system into the t-PDW state by pushing more opposite-spin pairing into the intra-branch pairing channel. A formal derivation of the energetics of the t-PDW state in the two limits of $r_{so} \rightarrow 0, \pi/2$ is provided in the Methods section.

Real space d -vectors for t-PDW states

We next study the solved pairing order parameters of all the states in the phase diagram, which helps to visualize the spatial modulation of the t-PDW state. As mentioned above,

the real space pairing order parameters can be compactly expressed by Eq. 1 as

$$\Delta_{i,\sigma\sigma'} = [(\psi_i\sigma_0 + \mathbf{d}_i \cdot \boldsymbol{\sigma})i\sigma_y]_{\sigma\sigma'}$$

Therefore, both the s -wave and p -wave components can be expressed as functions of the order parameters defined in Eq. 6. The mean-field t-PDW solution has four finite real order parameters as $(\Delta_{\parallel,Q}, \Delta_{\parallel,-Q}, \Delta_{\perp,Q} = -\Delta_{\perp,-Q})$ leading to the p -wave PDW states with the spatial modulated d -vector as

$$\begin{cases} d_{i,x} = -i(\Delta_{\parallel,Q} - \Delta_{\parallel,-Q}) \sin \left[Q(r_i + \frac{1}{2}) \right] \\ d_{i,y} = -i(\Delta_{\parallel,Q} + \Delta_{\parallel,-Q}) \cos \left[Q(r_i + \frac{1}{2}) \right] \\ d_{i,z} = -2i\Delta_{\perp,Q} \sin \left[Q(r_i + \frac{1}{2}) \right] \end{cases} \quad (8)$$

The real space d -vector is pure imaginary due to the time-reversal symmetry. The spatial modulation of a typical d -vector of the t-PDW state constructed from the pairing order parameters determined self-consistently with parameters $r_{so} = 1.4$ and $r_V = 0.3$ is shown schematically in Fig. 1, where the d -vector revolves around the origin in an elliptical orbit in 3D space within a period of the PDW state.

Moreover, the KFF state got for $r_{so} = 0$ and $r_V < 1$ has only one finite order parameter $\Delta_{\parallel,Q}$, corresponding to the d -vector as

$$\mathbf{d}_i = -i|\Delta_{\parallel,Q}| \left\{ \sin \left[Q(r_i + \frac{1}{2}) + \phi_{\parallel} \right], \cos \left[Q(r_i + \frac{1}{2}) + \phi_{\parallel} \right], 0 \right\}$$

with $\phi_{\parallel} = \arg(\Delta_{\parallel,Q})$. Then the revolving orbit of the d -vector around the origin becomes circular in the xy plane. The uniform MP solution has two finite order parameters with a complex $\Delta_{\perp,0}$ and pure imaginary $\Delta_{\parallel,0}$, which leads to the uniform pairing order parameter as $\psi_i = -\text{Re}[\Delta_{\perp,0}]$ and $\mathbf{d}_i = -\{\Delta_{\parallel,0}, 0, i\text{Im}[\Delta_{\perp,0}]\}$, which is shown schematically in the lower panel of Fig. 1.

Topological properties

The band dispersion of both t-PDW and MP states are shown in Fig. 4(a,c), both of which are fully gapped. In order to determine the topological properties of these states, we also calculate the end states of the finite-size systems for each phase. As shown in Fig. 4(b,d), both phases can host two pairs of Majorana zero modes (MZMs) indicating the nontrivial topological properties for both phases. Since the time-reversal symmetry is preserved for both phases, they can be classified as time-reversal invariant topological superconductors. The nontrivial topological property of the t-PDW state is easy to understand since it is a pure p -wave spin-triplet pairing state with d -vector given by Eq. 8 and the spatial modulation of the d -vector does not change its topological property. While for the MP state with both s -wave and p -wave pairing components, the state can be either topological superconductor or trivial superconductor [78]. For the chemical potential close to half-filling with $\mu = -0.4$, the MP state is always topological, which is labeled as MPTSC in the phase diagram of Fig. 3. However, a topological phase transition can occur when the chemical potential is tuned away from the half-filling, which is studied and discussed

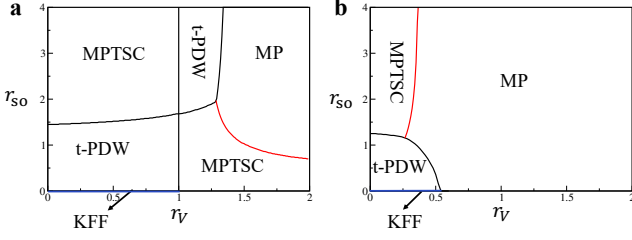


FIG. 5. **Phase diagrams away from half filling.** The chemical potential is set as $\mu = -1.4$ (a) and $\mu = -1.8$ (b) with all the other parameters unchanged. The KFF state is realized in the x -axis labeled by the bold blue line. The red lines represent the transition line between the TSC and trivial SC within the MP phase.

below.

Chemical potential effect

Finally, we also study the effect of the chemical potential on the phase diagram. The calculation above is done for $\mu = -0.4$ which is around the half-filling of the chain. We find that if the chemical potential is tuned away from the half-filling, the region for the t-PDW phase shrinks as shown in Fig. 5a with $\mu = -1.4$, and for μ close enough to the band top or bottom, the phase diagram changes dramatically, where the t-PDW state can only be realized for small values of r_V and r_{so} which is shown in Fig. 5b with $\mu = -1.8$.

The dramatic change of the phase diagram in Fig. 5b can be understood as follows. One important change in the phase diagrams is the absence of the vertical phase boundary with $r_V = 1$, where the finite momentum pairing state and uniform MP state are degenerate. We can first analyze these two degenerate states along this phase boundary. As shown in Eq. 7, along the whole phase boundary, the Hamiltonian is identical to the one with $\alpha_D = 0$ and $V_1 = V_2$ by choosing a proper spin quantization axis due to the remaining U(1) symmetry. Then we can perform a gauge transformation $c_{i\sigma} \rightarrow e^{i\sigma\theta_{\alpha}r_i}d_{i\sigma}$, and Eq. 7 becomes

$$\hat{H}_d = -t_{\alpha} \sum_{i\sigma} d_{i\sigma}^{\dagger} d_{i+1\sigma} + h.c. - V_1 \sum_{i\sigma\sigma'} n_{i\sigma}^d n_{i+1\sigma'}^d \quad (9)$$

where $t_{\alpha} = \sqrt{t^2 + \alpha_R^2 + \alpha_D^2}$, $\theta_{\alpha} = \arctan\left(\frac{\sqrt{\alpha_R^2 + \alpha_D^2}}{t}\right) = \frac{Q}{2}$ and $n_{i\sigma}^d = d_{i\sigma}^{\dagger} d_{i\sigma}$. Since the SOC is gauged away in the transformed Hamiltonian, which respects the full spin rotation and inversion symmetry, the ground state of such a system is either the uniform s -wave pairing state or the p -wave state with its d -vector pointing in any direction, depending on the chemical potential. For μ around the half filling, the Fermi points k_f are round $\pm\frac{\pi}{2}$ where the pairing function for the p -wave state $\Delta_p(k) \propto \sin k$ gains more energy than that of the s -wave state $\Delta_s(k) \propto \cos k$, making the p -wave pairing state as the ground state. On the other hand, if μ is sufficiently tuned away from the half-filling, the s -wave pairing will take over as k_f approaches $\pm\pi$, where $\Delta_s(k) \propto \cos k$ gains more energy.

We next undo the gauge transformation to see what these states are in the original basis. For the uniform p -wave state

in the transformed basis, the pairing order parameter in real space can be expressed as

$$\tilde{\Delta}_{i,\sigma\sigma'} = \langle d_{i\sigma} d_{i+1\sigma'} \rangle = [(\tilde{\mathbf{d}} \cdot \boldsymbol{\sigma}) i\sigma_y]_{\sigma\sigma'} \quad (10)$$

with $\tilde{\mathbf{d}}$ a pure imaginary constant vector. Then in the original basis, we have

$$\begin{aligned} \Delta_{i,\sigma\sigma'} &= \langle c_{i\sigma} c_{i+1\sigma'} \rangle = \langle d_{i\sigma} d_{i+1\sigma'} \rangle e^{i\theta_{\alpha}(\sigma r_i + \sigma' r_{i+1})} \\ &= \begin{cases} \tilde{\Delta}_{i,\sigma\sigma} e^{i\sigma Q(r_i + \frac{1}{2})}, & \text{if } \sigma' = \sigma \\ \tilde{\Delta}_{i,\sigma\bar{\sigma}} e^{-i\sigma \frac{Q}{2}}, & \text{if } \sigma' = \bar{\sigma} \end{cases} \end{aligned} \quad (11)$$

Therefore, if $\tilde{\mathbf{d}}$ is in the x - y plane corresponding to the equal-spin pairing, $\Delta_{i,\sigma\sigma} = \tilde{\Delta}_{i,\sigma\sigma} e^{i\sigma Q(r_i + \frac{1}{2})} = (-\tilde{d}_x \sigma + i\tilde{d}_y) e^{i\sigma Q(r_i + \frac{1}{2})}$. This pairing order parameter corresponds to the d -vector in the original basis as

$$\mathbf{d}_i = i|\tilde{\mathbf{d}}| \left\{ \sin \left[Q(r_i + \frac{1}{2}) + \phi_{\tilde{\mathbf{d}}} \right], \cos \left[Q(r_i + \frac{1}{2}) + \phi_{\tilde{\mathbf{d}}} \right], 0 \right\}$$

with $\phi_{\tilde{\mathbf{d}}} = \arctan\left(\frac{\tilde{d}_y}{\tilde{d}_x}\right)$, which is exactly the d -vector for the KFF state. On the other hand, if $\tilde{\mathbf{d}}$ is along the z direction corresponding to the opposite-spin pairing, $\Delta_{i,\sigma\bar{\sigma}} = \tilde{\Delta}_{i,\sigma\bar{\sigma}} e^{-i\sigma \frac{Q}{2}} = -\tilde{d}_z e^{-i\sigma \frac{Q}{2}}$. This corresponds to the uniform pairing order parameter with $\psi = -|\tilde{d}_z| \sin(\frac{Q}{2})$ and $\mathbf{d} = -i\{0, 0, |\tilde{d}_z| \cos(\frac{Q}{2})\}$, which describes the MP state. Therefore, the finite momentum pairing state and the uniform pairing state along the vertical phase boundary are mapped onto the p -wave pairing state with in-plane and out-of-plane d -vectors through a gauge transformation, which are always degenerate in energy. This means as long as μ is close to half-filling, the vertical phase boundary always exists as shown in Fig. 3 and Fig. 5a. On the other hand, if μ is close to the band top or bottom which leads to s -wave pairing ground state in the transformed basis with pairing order parameter $\tilde{\Delta}_{i,\sigma\sigma'} = \langle d_{i\sigma} d_{i+1\sigma'} \rangle = (\tilde{\psi} i\sigma_y)_{\sigma\sigma'}$, the states in the original basis become $\Delta_{i,\sigma\bar{\sigma}} = \tilde{\Delta}_{i,\sigma\bar{\sigma}} e^{-i\sigma \frac{Q}{2}} = \sigma \tilde{\psi} e^{-i\sigma \frac{Q}{2}}$, corresponding to the uniform MP state with pairing order parameters described by $\psi = \tilde{\psi} \cos(\frac{Q}{2})$ and $\mathbf{d} = -i\{0, 0, \tilde{\psi} \sin(\frac{Q}{2})\}$. In this case, there is no vertical phase boundary in the phase diagram, and only a small enough r_V can drive the system into a t-PDW state. Therefore, most parts of the phase diagram are occupied by the uniform MP state with the t-PDW state shrinking to the left bottom as shown in Fig. 5b.

Discussion

In this work, we systematically study the effective 1D model with mixed SOC and nearest-neighbor attraction. We find that the triplet pairing PDW state whose d -vector modulates in real space can be realized in this microscopic model. Moreover, the parameter region to realize such a PDW state is large when the chemical potential μ is close to half-filling and shrinks significantly when μ approaches the band top or bottom, which is accompanied by the existence of the topological phase transition within the MP state. This work introduces a simple and concrete theoretical model to realize

the PDW states and it also provides a possible explanation for the PDW state reported in the 1D domain wall of the iron-based superconductor Fe(Te,Se). We hope it stimulates the exploration of the PDW state in the embedded quantum structure of the high-temperature superconductors.

Methods

Two pairing channels

The two attraction terms in Eq. 2 can be written as

$$\begin{aligned} \hat{H}_I = & -\frac{V_1}{N_c} \sum_{k,k',q,\sigma} \sin k \sin k' c_{k+\frac{q}{2}\sigma}^\dagger c_{-k+\frac{q}{2}\sigma}^\dagger c_{-k'+\frac{q}{2}\sigma} c_{k'+\frac{q}{2}\sigma} \\ & - \frac{V_2}{N_c} \sum_{k,k',q,\sigma} e^{i(k-k')} c_{k+\frac{q}{2}\sigma}^\dagger c_{-k+\frac{q}{2}\sigma}^\dagger c_{-k'+\frac{q}{2}\sigma} c_{k'+\frac{q}{2}\sigma} \end{aligned} \quad (12)$$

which can be further decomposed into equal-spin and opposite-spin pairing channels as

$$\hat{H}_I = -N_c V_1 \sum_{q\sigma} \hat{\Delta}_{\parallel,q,\sigma}^\dagger \hat{\Delta}_{\parallel,q,\sigma} - N_c V_2 \sum_{q\sigma} \hat{\Delta}_{\perp,q,\sigma}^\dagger \hat{\Delta}_{\perp,q,\sigma} \quad (13)$$

$$\begin{aligned} \hat{H}_{MF} - \mu \hat{N} = & \sum_{k,\sigma,\sigma'} c_{k\sigma}^\dagger [(-2t \cos k - \mu)\sigma_0 - 2 \sin k (\alpha_R \sigma_z + \alpha_D \sigma_x)]_{\sigma\sigma'} c_{k\sigma'} - V_1 \sum_k (-i \sin k) (\Delta_{\parallel,0} c_{k\uparrow}^\dagger c_{-k\uparrow}^\dagger + \Delta_{\parallel,0}^* c_{k\downarrow}^\dagger c_{-k\downarrow}^\dagger) \\ & - V_1 \sum_k (-i \sin k) (\Delta_{\parallel,Q} c_{k+\frac{Q}{2}\uparrow}^\dagger c_{-k+\frac{Q}{2}\uparrow}^\dagger + \Delta_{\parallel,Q}^* c_{k-\frac{Q}{2}\downarrow}^\dagger c_{-k-\frac{Q}{2}\downarrow}^\dagger + \Delta_{\parallel,-Q} c_{k-\frac{Q}{2}\uparrow}^\dagger c_{-k-\frac{Q}{2}\uparrow}^\dagger + \Delta_{\parallel,-Q}^* c_{k+\frac{Q}{2}\downarrow}^\dagger c_{-k+\frac{Q}{2}\downarrow}^\dagger) \\ & - V_2 \sum_k (\Delta_{\perp,0} e^{ik} + \Delta_{\perp,0}^* e^{-ik}) c_{k+\frac{Q}{2}\uparrow}^\dagger c_{-k+\frac{Q}{2}\downarrow}^\dagger - V_2 \sum_k (\Delta_{\perp,-Q} e^{ik} + \Delta_{\perp,-Q}^* e^{-ik}) c_{k-\frac{Q}{2}\uparrow}^\dagger c_{-k-\frac{Q}{2}\downarrow}^\dagger \\ & - V_2 \sum_k (\Delta_{\perp,0} e^{ik} + \Delta_{\perp,0}^* e^{-ik}) c_{k\uparrow}^\dagger c_{-k\downarrow}^\dagger + h.c. + 2N_c [V_1 (|\Delta_{\parallel,0}|^2 + |\Delta_{\parallel,Q}|^2 + |\Delta_{\parallel,-Q}|^2) + V_2 (|\Delta_{\perp,0}|^2 + |\Delta_{\perp,Q}|^2 + |\Delta_{\perp,-Q}|^2)] \end{aligned} \quad (15)$$

The order parameters are determined self-consistently for a fixed chemical potential μ with the self-consistent equations

$$\begin{cases} \Delta_{\parallel,0} = \frac{1}{N_c} \sum_k i \sin k \langle c_{-k\uparrow} c_{k\uparrow} \rangle \\ \Delta_{\parallel,Q} = \frac{1}{N_c} \sum_k i \sin k \langle c_{-k+\frac{Q}{2}\uparrow} c_{k+\frac{Q}{2}\uparrow} \rangle \\ \Delta_{\parallel,-Q} = \frac{1}{N_c} \sum_k i \sin k \langle c_{-k-\frac{Q}{2}\uparrow} c_{k-\frac{Q}{2}\uparrow} \rangle \\ \Delta_{\perp,0} = \frac{1}{N_c} \sum_k e^{-ik} \langle c_{-k\downarrow} c_{k\uparrow} \rangle \\ \Delta_{\perp,Q} = \frac{1}{N_c} \sum_k e^{-ik} \langle c_{-k+\frac{Q}{2}\downarrow} c_{k+\frac{Q}{2}\uparrow} \rangle \\ \Delta_{\perp,-Q} = \frac{1}{N_c} \sum_k e^{-ik} \langle c_{-k-\frac{Q}{2}\downarrow} c_{k-\frac{Q}{2}\uparrow} \rangle \end{cases} \quad (16)$$

The self-consistent equations can be solved in the folded Brillouin Zone (BZ) for the commensurate Q , assuming $Q = \frac{\pi}{D}$, the BZ is folded into $\frac{1}{2D}$ of the original BZ. Then the mean-field Hamiltonian should be written in the Nambu ba-

where the pairing operators in the two channels are defined in Eq. 4, leading to the full Hamiltonian defined in Eq. 3.

Fermi surface of the bare bands

The non-interacting Hamiltonian $h_0(k)$ in Eq. 5 has eigenvalues correspond to the bare band dispersion as

$$\varepsilon_{k,s}^0 = -2t_\alpha \cos(k - s\theta_\alpha) - \mu, \quad s = \pm \quad (14)$$

with $t_\alpha = \sqrt{t^2 + \alpha_R^2 + \alpha_D^2}$ and $\theta_\alpha = \arctan\left(\frac{\sqrt{\alpha_R^2 + \alpha_D^2}}{t}\right) = \frac{Q}{2}$. The Fermi points are thus determined as $k_{f,s,\pm} = s\theta_\alpha \pm \arccos\left(-\frac{\mu}{2t_\alpha}\right)$ where $s = \pm$ corresponds to the two branches of the Fermi surfaces as shown schematically in Fig. 2.

Order parameters and mean-field Hamiltonian

After the mean-field decoupling using the ansatz defined by Eq. 6, the mean-field Hamiltonian can be written as

sis $\psi_k^\dagger = (c_{k+(n-1)Q\uparrow}^\dagger, c_{k+(n-1)Q\downarrow}^\dagger, c_{-k-(n-1)Q\uparrow}^\dagger, c_{-k-(n-1)Q\downarrow}^\dagger)$, with $n \in [1, 2D]$, as

$$\begin{aligned} \hat{H}_{MF} - \mu \hat{N} = & \frac{1}{4D} \sum_k \psi_k^\dagger h_k \psi_k + 2N_c [V_1 (|\Delta_{\parallel,0}|^2 + |\Delta_{\parallel,Q}|^2 + |\Delta_{\parallel,-Q}|^2) \\ & + V_2 (|\Delta_{\perp,0}|^2 + |\Delta_{\perp,Q}|^2 + |\Delta_{\perp,-Q}|^2)] - \mu N_c \end{aligned} \quad (17)$$

with h_k being the Hamiltonian matrix of size $8D$. Here, h_k can be written with the block form as

$$h_k = \begin{bmatrix} h_t(k, Q) & h_\Delta(k, Q) \\ h_\Delta^\dagger(k, Q) & -h_t^*(-k, -Q) \end{bmatrix} \quad (18)$$

where the non-zero elements of the matrices are,

$$h_t(k, Q)_{|2n-1:2n, 2n-1:2n} = h_0(k + (n-1)Q). \quad (19)$$

$$h_\Delta(k, Q)_{|2n-1:2n, 2n-1:2n} = \begin{bmatrix} 2iV_1 \Delta_{\parallel,0} \sin[k + (n-1)Q] & -V_2 (\Delta_{\perp,0} e^{i[k+(n-1)Q]} + \Delta_{\perp,0}^* e^{-i[k+(n-1)Q]}) \\ V_2 (\Delta_{\perp,0} e^{-i[k+(n-1)Q]} + \Delta_{\perp,0}^* e^{i[k+(n-1)Q]}) & 2iV_1 \Delta_{\parallel,0}^* \sin[k + (n-1)Q] \end{bmatrix} \quad (20)$$

$$h_{\Delta}(k, Q)_{(2n+1)';(2n+2)', 2n-1:2n} = \left[\begin{array}{cc} 2iV_1 \Delta_{\parallel, Q} \sin[k + (n - \frac{1}{2})Q] & -V_2 (\Delta_{\perp, Q} e^{i[k+(n-1/2)Q]} + \Delta_{\perp, -Q}^* e^{-i[k+(n-1/2)Q]}) \\ V_2 (\Delta_{\perp, Q} e^{-i[k+(n-1/2)Q]} + \Delta_{\perp, -Q}^* e^{i[k+(n-1/2)Q]}) & 2iV_1 \Delta_{\parallel, -Q}^* \sin[k + (n - \frac{1}{2})Q] \end{array} \right] \quad (21)$$

$$h_{\Delta}(k, Q)_{2n-1:2n, (2n+1)';(2n+2)'} = \left[\begin{array}{cc} 2iV_1 \Delta_{\parallel, -Q} \sin[k + (n - \frac{1}{2})Q] & -V_2 (\Delta_{\perp, Q}^* e^{-i[k+(n-1/2)Q]} + \Delta_{\perp, -Q} e^{i[k+(n-1/2)Q]}) \\ V_2 (\Delta_{\perp, Q}^* e^{i[k+(n-1/2)Q]} + \Delta_{\perp, -Q} e^{-i[k+(n-1/2)Q]}) & 2iV_1 \Delta_{\parallel, Q}^* \sin[k + (n - \frac{1}{2})Q] \end{array} \right] \quad (22)$$

for $n \in [1, 2D]$ and $(2n+1)' = (2n) \bmod (4D) + 1$ and $(2n+2)' = (2n+1) \bmod (4D) + 1$, so that all the indices are within the range of $[1, 4D]$.

Relation between the d -vectors and the order parameters

The real space pairing order parameters can be calculated as

$$\begin{cases} \Delta_{i,\uparrow\uparrow} = \langle c_{i\uparrow} c_{i+1\uparrow} \rangle = \Delta_{\parallel,0} + \Delta_{\parallel, Q} e^{iQ(r_i + \frac{1}{2})} + \Delta_{\parallel, -Q} e^{-iQ(r_i + \frac{1}{2})} \\ \Delta_{i,\downarrow\downarrow} = \langle c_{i\downarrow} c_{i+1\downarrow} \rangle = \Delta_{\parallel,0}^* + \Delta_{\parallel, Q}^* e^{-iQ(r_i + \frac{1}{2})} + \Delta_{\parallel, -Q}^* e^{iQ(r_i + \frac{1}{2})} \\ \Delta_{i,\uparrow\downarrow} = \langle c_{i\uparrow} c_{i+1\downarrow} \rangle = -\Delta_{\perp,0} - \Delta_{\perp, Q} e^{iQ(r_i + \frac{1}{2})} - \Delta_{\perp, -Q} e^{-iQ(r_i + \frac{1}{2})} \\ \Delta_{i,\downarrow\uparrow} = \langle c_{i\downarrow} c_{i+1\uparrow} \rangle = \Delta_{\perp,0}^* + \Delta_{\perp, Q}^* e^{-iQ(r_i + \frac{1}{2})} + \Delta_{\perp, -Q}^* e^{iQ(r_i + \frac{1}{2})} \end{cases} \quad (23)$$

Therefore, we can compactly express the pairing order parameters according to Eq. 1 as

$$\Delta_{i,\sigma\sigma'} = [(\psi_i \sigma_0 + \mathbf{d}_i \cdot \boldsymbol{\sigma}) i\sigma_y]_{\sigma\sigma'}$$

where ψ_i and \mathbf{d}_i correspond to the s -wave and p -wave components of the pairing order parameters and can be expressed as

$$\begin{cases} \psi_i = -\frac{1}{2} [(\Delta_{\perp,0} + \Delta_{\perp,0}^*) + (\Delta_{\perp, Q} + \Delta_{\perp, -Q}^*) e^{iQ(r_i + \frac{1}{2})} \\ \quad + (\Delta_{\perp, -Q} + \Delta_{\perp, Q}^*) e^{-iQ(r_i + \frac{1}{2})}] \\ d_{i,x} = -\frac{1}{2} [(\Delta_{\parallel,0} - \Delta_{\parallel,0}^*) + (\Delta_{\parallel, Q} - \Delta_{\parallel, -Q}^*) e^{iQ(r_i + \frac{1}{2})} \\ \quad + (\Delta_{\parallel, -Q} - \Delta_{\parallel, Q}^*) e^{-iQ(r_i + \frac{1}{2})}] \\ d_{i,y} = -\frac{i}{2} [(\Delta_{\parallel,0} + \Delta_{\parallel,0}^*) + (\Delta_{\parallel, Q} + \Delta_{\parallel, -Q}^*) e^{iQ(r_i + \frac{1}{2})} \\ \quad + (\Delta_{\parallel, -Q} + \Delta_{\parallel, Q}^*) e^{-iQ(r_i + \frac{1}{2})}] \\ d_{i,z} = -\frac{1}{2} [(\Delta_{\perp,0} - \Delta_{\perp,0}^*) + (\Delta_{\perp, Q} - \Delta_{\perp, -Q}^*) e^{iQ(r_i + \frac{1}{2})} \\ \quad + (\Delta_{\perp, -Q} - \Delta_{\perp, Q}^*) e^{-iQ(r_i + \frac{1}{2})}] \end{cases} \quad (24)$$

For the time-reversal symmetric states, ψ_i should be real, and \mathbf{d}_i should be imaginary.

Competition between finite momentum pairing and zero momentum pairing states

Since the finite (zero) momentum pairing states come from the intra-branch (inter-branch) pairing as shown in Fig. 2 and finite r_{so} mixes the spin components within the branch,

we can perform a change of basis as $\begin{pmatrix} c'_{i\uparrow} \\ c'_{i\downarrow} \end{pmatrix} = e^{i\theta\sigma_y} \begin{pmatrix} c_{i\uparrow} \\ c_{i\downarrow} \end{pmatrix}$

with $\theta = \arctan(r_{so})$, which aligns the spin quantization axis with the spin polarizations of the two branches of the non-interacting band. In this new basis, the non-interacting Hamiltonian becomes

$$h'_0(k) = -2t \cos k\sigma_0 - 2\sqrt{\alpha_R^2 + \alpha_D^2} \sin k\sigma_z \quad (25)$$

where the spin and the branch indices are locked so that the Fermi surface instability leads to finite momentum equal spin pairing and zero momentum opposite spin pairing. However, this makes the interacting part more complicated which reads

$$\begin{aligned} H'_I = & -V'_1 \sum_{i\sigma} n'_{i\sigma} n'_{i+1\sigma} - V'_2 \sum_{i\sigma} n'_{i\sigma} n'_{i+1\bar{\sigma}} \\ & + V'_{\theta 1} \sum_{i\sigma} (c'_{i\sigma}{}^\dagger c'_{i+1\sigma}{}^\dagger c'_{i+1\bar{\sigma}} c'_{i\bar{\sigma}} + c'_{i\sigma}{}^\dagger c'_{i+1\bar{\sigma}}{}^\dagger c'_{i+1\sigma} c'_{i\sigma}) \\ & + V'_{\theta 2} \sum_{i\sigma} [\sigma c'_{i\sigma}{}^\dagger c'_{i+1\sigma}{}^\dagger (c'_{i+1\sigma} c'_{i\bar{\sigma}} + c'_{i+1\bar{\sigma}} c'_{i\sigma}) + h.c.] \end{aligned} \quad (26)$$

where

$$\begin{cases} V'_1 = V_1 - \frac{1}{2}(V_1 - V_2) \sin^2 \theta \\ V'_2 = V_2 + \frac{1}{2}(V_1 - V_2) \sin^2 \theta \\ V'_{\theta 1} = -\frac{1}{2}(V_1 - V_2) \sin^2 \theta \\ V'_{\theta 2} = \frac{1}{4}(V_1 - V_2) \sin 2\theta \end{cases} \quad (27)$$

It is obvious that when $V_1 = V_2$ ($r_V = 1$), the interacting part is invariant under this U(1) spin rotation, and the finite momentum pairing state i.e., the KFF state and the MP state are degenerate as demonstrated in the previous section. When $r_V \neq 1$, this degeneracy is lifted and the ground state is determined by r_V and $\theta = \arctan(r_{so})$, leading to the phase diagram in Fig. 3.

We can understand how the finite momentum pairing state is favored in the two limits with $\theta \rightarrow 0$ and $\theta \rightarrow \pi/2$. When $\theta \rightarrow 0$, the two density-density term in Eq. 26 dominate and leads to the KFF state with order parameter $\Delta'_{\parallel, Q}$ when $r_V < 1$ since $V'_1 - V'_2 = (V_1 - V_2) \cos^2 \theta > 0$. The next order effect comes from the $V'_{\theta 1}$ term in Eq. 26, which can be written in the mean-field level as

$$H'_{I,\theta 1} = V'_{\theta 1} [\text{Re}(\Delta'_{\parallel, Q} \Delta'_{\parallel, -Q}) - \text{Re}(\Delta_{\perp, 0}^2)]. \quad (28)$$

This term induces a small amount of KFF state $\Delta'_{\parallel, -Q}$ leading to the t-PDW state. The $V'_{\theta 2}$ term induces a spin-triplet pairing with opposite spin components. When $\theta \rightarrow \pi/2$, we have $V'_1 \approx V'_2$ and $V'_{\theta 2} \approx 0$, which means it is $H'_{I,\theta 1}$ that lifts the degeneracy of the finite momentum and zero momentum pairing state and determines the ground state. As demonstrated in the previous section, the zero momentum MP state in this limit has the order parameter $\Delta'_{\perp, 0} \propto i e^{-iQ/2}$ leading to $\text{Re}(\Delta_{\perp, 0}^2) \propto -\cos Q < 0$. Considering the relation $|\Delta'_{\parallel, Q}| \approx |\Delta'_{\perp, 0}| > |\Delta'_{\parallel, -Q}|$ in this limit, we can conclude that the t-PDW state gains more energy when $V'_{\theta 1} > 0$ i.e., $r_V > 1$ and the MP state becomes the ground state when $V'_{\theta 1} < 0$

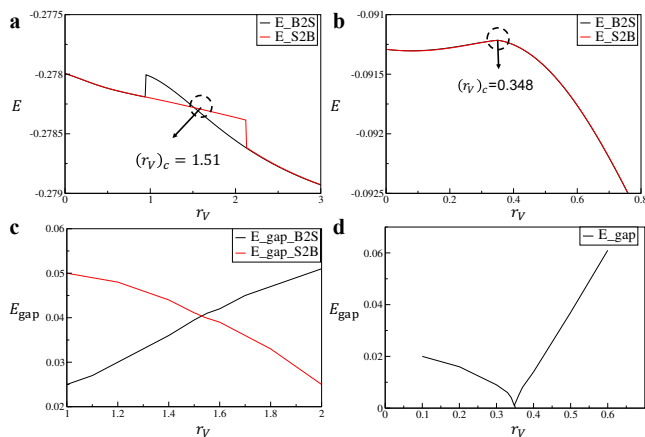


FIG. 6. **Topological phase transitions within the MP states.** **a,b** The evolution of the total energy across the phase boundary between the topological trivial and non-trivial MP states shown in Fig. 3b,c with the fixed value of $r_{so} = 1.0$ and $\mu = -1.4$ for **a** and $r_{so} = 3.0$ and $\mu = -1.8$ for **b**. Here, the black (red) line corresponds to tuning r_V from big (small) to small (big) values, and the hysteresis behavior in **a** indicates the 1st-order character of the phase transition. **c,d** The evolution of the extracted band gap of the states across the corresponding phase boundary described in **a,b**. The band gap never closes for the case with $\mu = -1.4$ (**c**) and closes and reopens across the phase boundary with the critical value $r_V = 0.348$ for the case with $\mu = -1.8$ (**d**).

i.e., $r_V < 1$, which explains the main phase diagram shown in Fig. 3.

Topological phase transition within the MP state away from half-filling

Another feature of the phase diagram when the chemical potential is tuned away from the half-filling is the existence of an extra topological phase transition within the MP state with

the phase boundary represented by the red lines in Fig. 5a and Fig. 5b. These phase boundaries separate the topological superconductor and the trivial superconductor, whose topological property can be determined by a Z_2 invariant \mathcal{N} [80], which was used to study the topological phase diagram in the atomic line defect [78].

We carefully study the phase transitions for these two cases. We find that for $\mu = -1.4$ where the vertical phase boundary mentioned above still exists, the topological phase transition is first-order. To see it more transparently, we fix the ratio $r_{so} = 1.0$ and tune the parameter r_V through the phase boundary. We find the total energy has a hysteresis behavior as the parameter r_V is tuned from big to small values and the small to big values respectively which is shown in Fig. 6a, indicating the first-order feature of the transition. Moreover, the band structure of the TSC and trivial SC state are almost identical close to the transition point and the band gap of the system never closes across the phase transition as shown in Fig. 6c.

As the chemical potential is further tuned towards the band bottom with $\mu = -1.8$, besides the dramatic change of the phase diagram discussed above, the topological phase transition within the MP state also switches from first-order to continuous. As an example, we again fix the ratio $r_{so} = 3.0$ and tune the parameter r_V through the phase boundary. In this case, the total energy does not show any hysteresis behavior as shown in Fig. 6b. We further calculate the band dispersion of the state as the parameters are tuned across the phase boundary, which shows a typical gap close-and-reopen behavior across the topological phase transition as shown in Fig. 6d.

Acknowledgments

YZ is supported in part by National Natural Science Foundation of China (NSFC) Grants No. 12074276 and No. 12274279. ZW is supported by the U.S. Department of Energy, Basic Energy Sciences, Grant No. DE FG02-99ER45747.

-
- [1] J. Bardeen, L. N. Cooper, and J. R. Schrieffer, Theory of superconductivity, *Phys. Rev.* **108**, 1175 (1957).
 - [2] P. Fulde and R. A. Ferrell, Superconductivity in a strong spin-exchange field, *Phys. Rev.* **135**, A550 (1964).
 - [3] A. Larkin and Y. Ovchinnikov, Nonuniform state of superconductors, *Sov. Phys. JETP* **20**, 762 (1965).
 - [4] M. Smidman, M. B. Salamon, H. Q. Yuan, and D. F. Agterberg, Superconductivity and spin-orbit coupling in noncentrosymmetric materials: a review, *Reports on Progress in Physics* **80**, 036501 (2017).
 - [5] L. P. Gor'kov and E. I. Rashba, Superconducting 2d system with lifted spin degeneracy: Mixed singlet-triplet state, *Phys. Rev. Lett.* **87**, 037004 (2001).
 - [6] V. Barzykin and L. P. Gor'kov, Inhomogeneous stripe phase revisited for surface superconductivity, *Phys. Rev. Lett.* **89**, 227002 (2002).
 - [7] D. Agterberg, Novel magnetic field effects in unconventional superconductors, *Physica C: Superconductivity* **387**, 13 (2003), proceedings of the 3rd Polish-US Workshop on Superconductivity and Magnetism of Advanced Materials.
 - [8] O. V. Dimitrova and M. V. Feigel'man, Phase diagram of a surface superconductor in parallel magnetic field, *Journal of Experimental and Theoretical Physics Letters* **78**, 637 (2003).
 - [9] R. P. Kaur, D. F. Agterberg, and M. Sigrist, Helical vortex phase in the noncentrosymmetric CePt_3Si , *Phys. Rev. Lett.* **94**, 137002 (2005).
 - [10] D. F. Agterberg and R. P. Kaur, Magnetic-field-induced helical and stripe phases in rashba superconductors, *Phys. Rev. B* **75**, 064511 (2007).
 - [11] O. Dimitrova and M. V. Feigel'man, Theory of a two-dimensional superconductor with broken inversion symmetry, *Phys. Rev. B* **76**, 014522 (2007).
 - [12] K. V. Samokhin, Upper critical field in noncentrosymmetric superconductors, *Phys. Rev. B* **78**, 224520 (2008).
 - [13] Y. Yanase and M. Sigrist, Helical superconductivity in noncentrosymmetric superconductors with dominantly spin triplet pairing, *Journal of the Physical Society of Japan* **77**, 342 (2008).
 - [14] K. Michaeli, A. C. Potter, and P. A. Lee, Superconducting and ferromagnetic phases in $\text{SrTiO}_3/\text{LaAlO}_3$ oxide interface structures: Possibility of finite momentum pairing, *Phys. Rev. Lett.* **108**,

- 117003 (2012).
- [15] T. Sekihara, R. Masutomi, and T. Okamoto, Two-dimensional superconducting state of monolayer pb films grown on $\text{GaS}(110)$ in a strong parallel magnetic field, *Phys. Rev. Lett.* **111**, 057005 (2013).
- [16] M. Houzet and J. S. Meyer, Quasiclassical theory of disordered rashba superconductors, *Phys. Rev. B* **92**, 014509 (2015).
- [17] N. F. Q. Yuan and L. Fu, Topological metals and finite-momentum superconductors, *Proceedings of the National Academy of Sciences* **118**, e2019063118 (2021).
- [18] M. Davydova, S. Prembabu, and L. Fu, Universal josephson diode effect, *Science Advances* **8**, eabo0309 (2022).
- [19] A. Daido, Y. Ikeda, and Y. Yanase, Intrinsic superconducting diode effect, *Phys. Rev. Lett.* **128**, 037001 (2022).
- [20] Y. Zhang and Z. Wang, Kramers fulde-ferrell state and superconducting spin diode effect, *Phys. Rev. B* **107**, 224510 (2023).
- [21] D. F. Agterberg, J. S. Davis, S. D. Edkins, E. Fradkin, D. J. Van Harlingen, S. A. Kivelson, P. A. Lee, L. Radzihovsky, J. M. Tranquada, and Y. Wang, The physics of pair-density waves: Cuprate superconductors and beyond, *Annual Review of Condensed Matter Physics* **11**, 231 (2020).
- [22] Q. Li, M. Hücker, G. D. Gu, A. M. Tsvelik, and J. M. Tranquada, Two-dimensional superconducting fluctuations in stripe-ordered $\text{La}_{1.875}\text{Ba}_{0.125}\text{CuO}_4$, *Phys. Rev. Lett.* **99**, 067001 (2007).
- [23] E. Berg, E. Fradkin, E.-A. Kim, S. A. Kivelson, V. Oganesyan, J. M. Tranquada, and S. C. Zhang, Dynamical layer decoupling in a stripe-ordered high- T_c superconductor, *Phys. Rev. Lett.* **99**, 127003 (2007).
- [24] D. F. Agterberg and H. Tsunetsugu, Dislocations and vortices in pair-density-wave superconductors, *Nature Physics* **4**, 639 (2008).
- [25] E. Berg, E. Fradkin, and S. A. Kivelson, Charge-4e superconductivity from pair-density-wave order in certain high-temperature superconductors, *Nature Physics* **5**, 830 (2009).
- [26] E. Fradkin, S. A. Kivelson, and J. M. Tranquada, Colloquium: Theory of intertwined orders in high temperature superconductors, *Rev. Mod. Phys.* **87**, 457 (2015).
- [27] M. H. Hamidian, S. D. Edkins, S. H. Joo, A. Kostin, H. Eisaki, S. Uchida, M. J. Lawler, E. A. Kim, A. P. Mackenzie, K. Fujita, J. Lee, and J. C. S. Davis, Detection of a cooper-pair density wave in $\text{Bi}_2\text{Sr}_2\text{CaCu}_2\text{O}_{8+x}$, *Nature* **532**, 343 (2016).
- [28] W. Ruan, X. Li, C. Hu, Z. Hao, H. Li, P. Cai, X. Zhou, D.-H. Lee, and Y. Wang, Visualization of the periodic modulation of cooper pairing in a cuprate superconductor, *Nature Physics* **14**, 1178 (2018).
- [29] S. D. Edkins, A. Kostin, K. Fujita, A. P. Mackenzie, H. Eisaki, S. Uchida, S. Sachdev, M. J. Lawler, E.-A. Kim, J. C. S. Davis, and M. H. Hamidian, Magnetic field-induced pair density wave state in the cuprate vortex halo, *Science* **364**, 976 (2019).
- [30] X. Li, C. Zou, Y. Ding, H. Yan, S. Ye, H. Li, Z. Hao, L. Zhao, X. Zhou, and Y. Wang, Evolution of charge and pair density modulations in overdoped $\text{Bi}_2\text{Sr}_2\text{CuO}_{6+\delta}$, *Phys. Rev. X* **11**, 011007 (2021).
- [31] Z. Du, H. Li, S. H. Joo, E. P. Donoway, J. Lee, J. C. S. Davis, G. Gu, P. D. Johnson, and K. Fujita, Imaging the energy gap modulations of the cuprate pair-density-wave state, *Nature* **580**, 65 (2020).
- [32] H.-D. Chen, O. Vafek, A. Yazdani, and S.-C. Zhang, Pair density wave in the pseudogap state of high temperature superconductors, *Phys. Rev. Lett.* **93**, 187002 (2004).
- [33] P. A. Lee, Amperean pairing and the pseudogap phase of cuprate superconductors, *Phys. Rev. X* **4**, 031017 (2014).
- [34] E. Berg, E. Fradkin, and S. A. Kivelson, Pair-density-wave correlations in the kondo-heisenberg model, *Phys. Rev. Lett.* **105**, 146403 (2010).
- [35] A. Jaefari and E. Fradkin, Pair-density-wave superconducting order in two-leg ladders, *Phys. Rev. B* **85**, 035104 (2012).
- [36] J. Venderley and E.-A. Kim, Evidence of pair-density wave in spin-valley locked systems, *Science Advances* **5**, eaat4698 (2019).
- [37] Y.-H. Zhang and A. Vishwanath, Pair-density-wave superconductor from doping haldane chain and rung-singlet ladder, *Phys. Rev. B* **106**, 045103 (2022).
- [38] H.-C. Jiang, Pair density wave in the doped three-band hubbard model on two-leg square cylinders, *Phys. Rev. B* **107**, 214504 (2023).
- [39] F. Chen and D. N. Sheng, Singlet, triplet, and pair density wave superconductivity in the doped triangular-lattice moiré system, *Phys. Rev. B* **108**, L201110 (2023).
- [40] X. Y. Xu, K. T. Law, and P. A. Lee, Pair density wave in the doped $t-j$ model with ring exchange on a triangular lattice, *Phys. Rev. Lett.* **122**, 167001 (2019).
- [41] C. Peng, Y.-F. Jiang, T. P. Devereaux, and H.-C. Jiang, Precursor of pair-density wave in doping kitaev spin liquid on the honeycomb lattice, *npj Quantum Materials* **6**, 64 (2021).
- [42] K. S. Huang, Z. Han, S. A. Kivelson, and H. Yao, Pair-density-wave in the strong coupling limit of the holstein-hubbard model, *npj Quantum Materials* **7**, 17 (2022).
- [43] H.-C. Jiang and T. P. Devereaux, Pair density wave and superconductivity in a kinetically frustrated doped Emery model on a square lattice, *arXiv e-prints*, arXiv:2309.11786 (2023).
- [44] Y.-F. Jiang and H. Yao, Pair density wave superconductivity: a microscopic model in two dimensions, *arXiv e-prints*, arXiv:2308.08609 (2023).
- [45] S. Zhou and Z. Wang, Chern fermi pocket, topological pair density wave, and charge-4e and charge-6e superconductivity in kagomé superconductors, *Nature Communications* **13**, 7288 (2022).
- [46] A. Himeda, T. Kato, and M. Ogata, Stripe states with spatially oscillating d -wave superconductivity in the two-dimensional $t-t'-j$ model, *Phys. Rev. Lett.* **88**, 117001 (2002).
- [47] M. Raczkowski, M. Capello, D. Poilblanc, R. Frésard, and A. M. Oleś, Unidirectional d -wave superconducting domains in the two-dimensional $t-j$ model, *Phys. Rev. B* **76**, 140505 (2007).
- [48] A. Aperis, G. Varelogiannis, P. B. Littlewood, and B. D. Simons, Coexistence of spin density wave, d -wave singlet and staggered π -triplet superconductivity, *Journal of Physics: Condensed Matter* **20**, 434235 (2008).
- [49] K.-Y. Yang, W. Q. Chen, T. M. Rice, M. Sigrist, and F.-C. Zhang, Nature of stripes in the generalized $t-j$ model applied to the cuprate superconductors, *New Journal of Physics* **11**, 055053 (2009).
- [50] F. Loder, S. Graser, A. P. Kampf, and T. Kopp, Mean-field pairing theory for the charge-stripe phase of high-temperature cuprate superconductors, *Phys. Rev. Lett.* **107**, 187001 (2011).
- [51] G. Y. Cho, J. H. Bardarson, Y.-M. Lu, and J. E. Moore, Superconductivity of doped weyl semimetals: Finite-momentum pairing and electronic analog of the $^3\text{He}-a$ phase, *Phys. Rev. B* **86**, 214514 (2012).
- [52] R. Soto-Garrido, G. Y. Cho, and E. Fradkin, Quasi-one-dimensional pair density wave superconducting state, *Phys. Rev. B* **91**, 195102 (2015).
- [53] Y. Wang, D. F. Agterberg, and A. Chubukov, Coexistence of charge-density-wave and pair-density-wave orders in underdoped cuprates, *Phys. Rev. Lett.* **114**, 197001 (2015).
- [54] S.-K. Jian, Y.-F. Jiang, and H. Yao, Emergent spacetime supersymmetry in 3d weyl semimetals and 2d dirac semimetals,

- Phys. Rev. Lett.* **114**, 237001 (2015).
- [55] J. Wårdh and M. Granath, Effective model for a supercurrent in a pair-density wave, *Phys. Rev. B* **96**, 224503 (2017).
- [56] J. Wårdh, B. M. Andersen, and M. Granath, Suppression of superfluid stiffness near a Lifshitz-point instability to finite-momentum superconductivity, *Phys. Rev. B* **98**, 224501 (2018).
- [57] Z. Han, S. A. Kivelson, and H. Yao, Strong coupling limit of the Holstein-Hubbard model, *Phys. Rev. Lett.* **125**, 167001 (2020).
- [58] D. Chakraborty and A. M. Black-Schaffer, Odd-frequency pair density wave correlations in underdoped cuprates, *New Journal of Physics* **23**, 033001 (2021).
- [59] C. Setty, J. Zhao, L. Fanfarillo, E. W. Huang, P. J. Hirschfeld, P. W. Phillips, and K. Yang, Exact solution for finite center-of-mass momentum Cooper pairing, *Phys. Rev. B* **108**, 174506 (2023).
- [60] J.-T. Jin, K. Jiang, H. Yao, and Y. Zhou, Interplay between pair density wave and a nested Fermi surface, *Phys. Rev. Lett.* **129**, 167001 (2022).
- [61] J.-J. Miao, F.-C. Zhang, and Y. Zhou, Instability of three-band Tomonaga-Luttinger liquid: Renormalization group analysis and possible application to $\text{K}_2\text{Cr}_3\text{As}_3$, *Phys. Rev. B* **94**, 205129 (2016).
- [62] Z. Han and S. A. Kivelson, Pair density wave and reentrant superconducting tendencies originating from valley polarization, *Phys. Rev. B* **105**, L100509 (2022).
- [63] P. Coleman, A. Panigrahi, and A. Tsvelik, Solvable 3d kondo lattice exhibiting pair density wave, odd-frequency pairing, and order fractionalization, *Phys. Rev. Lett.* **129**, 177601 (2022).
- [64] D. Shaffer, F. J. Burnell, and R. M. Fernandes, Weak-coupling theory of pair density wave instabilities in transition metal dichalcogenides, *Phys. Rev. B* **107**, 224516 (2023).
- [65] D. Shaffer and L. H. Santos, Triplet pair density wave superconductivity on the π -flux square lattice, *Phys. Rev. B* **108**, 035135 (2023).
- [66] Y.-M. Wu, Z. Wu, and H. Yao, Pair-density-wave and chiral superconductivity in twisted bilayer transition metal dichalcogenides, *Phys. Rev. Lett.* **130**, 126001 (2023).
- [67] Y.-M. Wu, P. A. Nosov, A. A. Patel, and S. Raghu, Pair density wave order from electron repulsion, *Phys. Rev. Lett.* **130**, 026001 (2023).
- [68] T. Schwemmer, H. Hohmann, M. Dürrnagel, J. Potten, J. Beyer, S. Rachel, Y.-M. Wu, S. Raghu, T. Müller, W. Hanke, and R. Thomale, Pair Density Wave Instability in the Kagome Hubbard Model, *arXiv e-prints*, arXiv:2302.08517 (2023).
- [69] G. Jiang and Y. Barlas, Pair density waves from local band geometry, *Phys. Rev. Lett.* **131**, 016002 (2023).
- [70] C. Setty, L. Fanfarillo, and P. J. Hirschfeld, Mechanism for fluctuating pair density wave, *Nature Communications* **14**, 3181 (2023).
- [71] H. Zhao, R. Blackwell, M. Thinel, T. Handa, S. Ishida, X. Zhu, A. Iyo, H. Eisaki, A. N. Pasupathy, and K. Fujita, Smectic pair-density-wave order in eurbfe4as4 , *Nature* **618**, 940 (2023).
- [72] Y. Liu, T. Wei, G. He, Y. Zhang, Z. Wang, and J. Wang, Pair density wave state in a monolayer high- T_c iron-based superconductor, *Nature* **618**, 934 (2023).
- [73] Q. Gu, J. P. Carroll, S. Wang, S. Ran, C. Broyles, H. Siddiquee, N. P. Butch, S. R. Saha, J. Paglione, J. C. S. Davis, and X. Liu, Detection of a pair density wave state in ute_2 , *Nature* **618**, 921 (2023).
- [74] A. Aishwarya, J. May-Mann, A. Raghavan, L. Nie, M. Romanelli, S. Ran, S. R. Saha, J. Paglione, N. P. Butch, E. Fradkin, and V. Madhavan, Magnetic-field-sensitive charge density waves in the superconductor ute_2 , *Nature* **618**, 928 (2023).
- [75] H. Chen, H. Yang, B. Hu, Z. Zhao, J. Yuan, Y. Xing, G. Qian, Z. Huang, G. Li, Y. Ye, S. Ma, S. Ni, H. Zhang, Q. Yin, C. Gong, Z. Tu, H. Lei, H. Tan, S. Zhou, C. Shen, X. Dong, B. Yan, Z. Wang, and H.-J. Gao, Roton pair density wave in a strong-coupling kagome superconductor, *Nature* **599**, 222 (2021).
- [76] H. Deng, H. Qin, G. Liu, T. Yang, R. Fu, Z. Zhang, X. Wu, Z. Wang, Y. Shi, J. Liu, H. Liu, X.-Y. Yan, W. Song, X. Xu, Y. Zhao, M. Yi, G. Xu, H. Hohmann, S. C. Holbæk, M. Dürrnagel, S. Zhou, G. Chang, Y. Yao, Q. Wang, Z. Guguchia, T. Neupert, R. Thomale, M. H. Fischer, and J.-X. Yin, Chiral kagome superconductivity modulations with residual Fermi arcs, *Nature* **632**, 775 (2024).
- [77] M. Sigrist and K. Ueda, Phenomenological theory of unconventional superconductivity, *Rev. Mod. Phys.* **63**, 239 (1991).
- [78] Y. Zhang, K. Jiang, F. Zhang, J. Wang, and Z. Wang, Atomic line defects and topological superconductivity in unconventional superconductors, *Phys. Rev. X* **11**, 011041 (2021).
- [79] C. Chen, K. Jiang, Y. Zhang, C. Liu, Y. Liu, Z. Wang, and J. Wang, Atomic line defects and zero-energy end states in monolayer $\text{Fe}(\text{Te},\text{Se})$ high-temperature superconductors, *Nature Physics* **16**, 536 (2020).
- [80] X.-L. Qi, T. L. Hughes, and S.-C. Zhang, Topological invariants for the Fermi surface of a time-reversal-invariant superconductor, *Phys. Rev. B* **81**, 134508 (2010).